Investigation of size, surface charge, PEGylation degree and concentration on the cellular uptake of polymer nanoparticles

Raffaele Ferrari [a], Monica Lupi [b], Claudio Colombo [a], Massimo Morbidelli [c], Maurizio D'Incalci [b], Davide Moscatelli [a,*]

[a] *Department of Chemistry, Materials and Chemical Engineering, Politecnico di Milano, Via Mancinelli 7, 20131 Milano, Italy*
[b] *Department of Oncology, IRCCS – Istituto di Ricerche Farmacologiche Mario Negri, Via La Masa 19, 20156 Milano, Italy*
[c] *Institute for Chemical and Bioengineering, ETH Zurich, CH-8093 Zurich, Switzerland*

Received 4 March 2014
Received in revised form
21 September 2014
Accepted 2 October 2014
Available online 13 October 2014

1. Introduction

Cellular uptake studies of polymersomes, polymer micelles and nanoparticles (NPs) are significantly growing in terms of number and quality during the last years [1–3], leading to a substantial improvement of the internalization mechanism comprehension [4,5]. In particular, many efforts have been carried out in order to increase the accuracy of *in vitro* measurements of cellular uptake; moving from a relative to an absolute quantification of NPs internalized into cells thus leading to a more accurate comparison between different NP formulations [6–8]. Then, the optimization of the polymer NP production step, aiming to ensure the highest uptake maintaining low cell death levels, is becoming a challenging field of research [9,10]. Indeed, uptake experiments are performed in well evaluable and reproducible conditions, and the comparison between NPs with different formulations and characteristics appears as an easy optimization step before *in vivo* or further *in vitro* experiments [10]. With this goal, in the field of polymer NPs, a lot of works recently appeared in literature aiming to elucidate the role of size [11–14], PEGylation [15,16], charge surface [6,15,17], presence of emulsifier [18], shape [19,20], and core material [21–23] on the NP internalization.

Here, we produced a wide range of polymer NPs in order to systematically evaluate their uptake adopting an analytical method recently proposed in the literature, which allows a more detailed and affordable data comparison [8]. In particular, the adopted method allows the estimation of the mean number of fluorescent NPs internalized in each cell excluding the contribution coming from dead cells and non-internalized aggregated NPs. Rhodamine B (RhB) covalently bonded to the polymer matrix has been adopted as a fluorescent dye to reveal the presence of NPs [24], in order to unambiguously detect them thus avoiding problems due to the dye diffusion out of the NPs [25]. All of the different NPs have been produced through emulsion free radical polymerization processes using poly(methyl methacrylate) for the synthesis of non-biodegradable NPs, and both poly(ε-caprolactone) (PCL) and

* Corresponding author. Tel.: +39 02 2399 3135.
E-mail address: davide.moscatelli@polimi.it (D. Moscatelli).

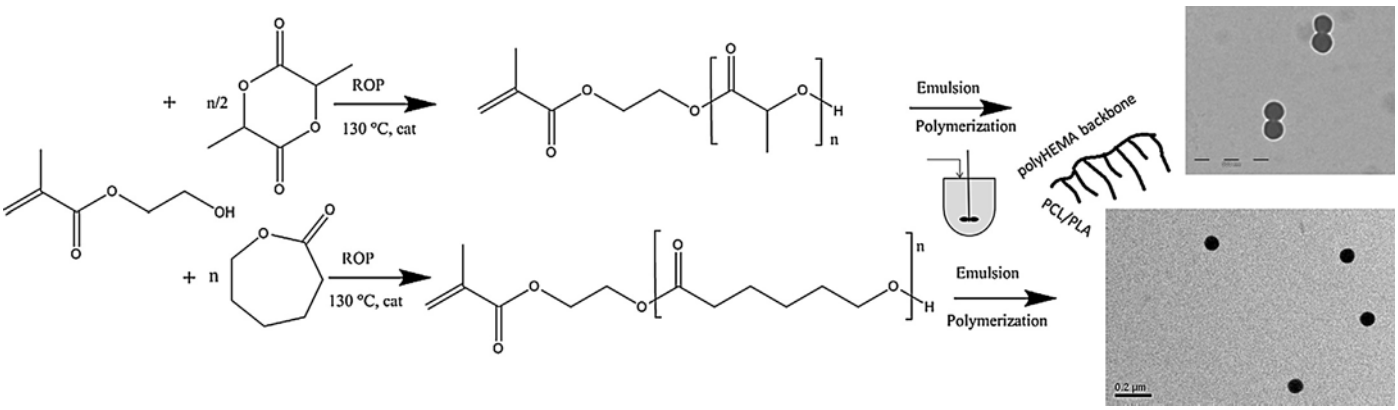

Scheme 1. Graphical representation of the reactive pathway adopted to obtain the PLA-based NPs (TEM of batch #2, upper image) and PCL-based NPs (TEM of batch #7, lower image).

poly(lactic acid) (PLA) – based polymers for biodegradable ones. NP synthesis procedures allow obtaining NPs with a fine control of size, particle size distribution, and ζ potential. In particular, the non-biodegradable PMMA NPs were easily obtained by emulsion polymerization, while for the biodegradable NPs a two-step process was exploited as graphically reported in Scheme 1. First, ring opening polymerization was used to produce macromonomers constituted of short PLA or PCL chains functionalized with HEMA vinyl end group and thus suitable for free radical polymerization. The next emulsion free radical polymerization step gives NPs with a peculiar comb-like structure, where a poly(2-hydroxy-ethyl methacrylate) backbone is grafted with polyester chains with controllable length [26,27]. Moreover, the emulsion polymerization allows an easy functionalization of the PEG chains or fixed charges which are covalently linked to the NPs during the polymer synthesis [28,29]. These materials were then selected to produce NPs with different features in terms of size, surface charge, PEGylation, presence of emulsifier, and macromonomer molecular weight (MW). As it is well known that NP internalization strongly depends on the cell system as well as that the amount of internalized NPs can be affected by the cellular concentration [7,30], all the *in vitro* experiments have been performed adopting a single tumor cell line and standardizing the culture conditions. More in detail 4T1 cells have been selected as a good model for breast cancer cells [31]. This choice can be made without losing generality since, without active targeting, obtained *in vitro* results can be extended to different types of cancer cells after applying a suitable scaling while other types of cells can be subjected to different internalization mechanisms. The reference time adopted for internalization experiments was fixed to 24 h and the obtained results were expressed as an average number of NPs internalized in each cell as a function of NP size or concentration. This was aimed to have a direct comparison of the different NP formulations and then to assess the contribution of different parameters to the uptake process. Additional experiments were also performed at short or longer incubation time in order to distinguish the entry mechanism of NPs and their washout; depending upon aforementioned NP features.

Since various NPs were produced, their potential cytostatic and cytotoxic effects were also verified by counting the cells at the end of the incubation (24 h). The results coming from this measurement were coupled with the uptake efficiency aiming to establish a criterion to select NPs which guarantee a negligible effect on cell proliferation ensuring high uptake efficiency and, for drug delivery purposes, a higher amount of drug loaded into NPs and, consequently, internalized into cells.

2. Experimental

2.1. Nanoparticle synthesis

As reported in Section 1, all of the NPs were produced through emulsion free radical polymerization. Macromonomers constituted of polymer chains (PLA or PCL) with controllable average chain length, ranging from 3 to 10, functionalized with 2-hydroxyethyl methacrylate (HEMA) vinyl end group were produced; namely HEMA-CL_3, HEMA-LA_6, HEMA-LA_8, and HEMA-LA_{10}. They were obtained through a ring opening polymerization (ROP) adopting a procedure reported in literature [26,27]. Similarly, fluorescent HEMA-RhB macromonomer was synthesized as already described [24]. Detailed macromonomer characterization is reported in the Supplementary information (SI) section. All the biodegradable NPs were produced following an emulsion polymerization process, as already described [26,32], and adopting macromonomers produced as described above. Briefly, all the surfactant free PLA-based NPs were produced adopting a monomer starved semi batch polymerization (MSSEP) process where the more hydrophilic monomer, constituted of PEG chains functionalized with a vinyl end group (HEMA-PEG_{19}), was previously loaded into the reactor and the hydrophobic one was slowly fed into the reactor. PCL-based NPs were produce through a MSSEP or batch emulsion polymerization (BEP) process performed in different experimental conditions in order to produce NPs with different characteristics. In particular, a PEGylated macromonomer (HEMA-PEG_9) was adopted along with the PCL-based one and the amounts of both HEMA-PEG_9 and HEMA-PEG_{19} were properly varied in order to produce NPs with different PEGylation degree. NPs with different emulsifiers were also produced (*i.e.* Tween80 and SDS). Surfactant free NPs with a positive charge distributed along the NP surface were obtained adopting a positively charged surfmer, [2-(methacryloyloxy)ethyl] trimethylammonium chloride (HEMA-Ch or Ch) using both HEMA-CL_3 and MMA as monomers. Finally, by varying the initiator and the amount of emulsifier, as well as synthesis condition, PMMA-based NPs with precisely controlled size (50, 100, and 200 nm) were obtained both *via* BEP and MSSEP processes. Detailed synthesis for each NP is reported in the SI section. After the synthesis, NPs are characterized in terms of average diameter and particle size distribution by dynamic light scattering (Malvern, Zetanano ZS) using the cumulant method as defined by ISO (standard document 13321:1996E), all the reported data are an average between three measures of the same sample. TEM analyses have been performed. TEM images were obtained using a 200 kV electron microscope (Philips CM200-FEG) and preparing the sample drying a drop of

NPs latex on a copper grid coated with a carbon film (Cu-grid 200 Mash).

2.2. Cell culture and NP uptake

4T1 cell line, derived from a mouse mammary tumor, were grown in high glucose DMEM/F12 (Biowest, Nuaillé, France) supplemented with 10% fetal bovine serum (Lonza, Basel, Switzerland) and 2% L-glutamine (Biowest) and maintained at 37 °C in a humidified atmosphere containing 5% CO_2. Cells were grown as monolayers in T25 tissue flasks and routinely subcultured twice weekly, detaching them using 1 ml 0.05% trypsin-0.02% EDTA in PBS (Biowest). Trypsin activity was stopped using culture medium.

4T1 cells were seeded at the concentration of 10,000 cell/ml; then, 24 h after seeding, were exposed to different NP concentrations. At the end of the incubation (24 h, for uptake studies; 2, 5, 8 and 24 h for kinetics internalization study), cells were harvested and cell suspensions were split in three aliquots, for absolute count using a Coulter Counter ZM (Coulter Electronics, UK), plate fluorimetry and flow cytometry measures. At least three replicated wells were used for each concentration and time in all experiments.

2.3. Analysis of NP uptake

NP uptake has been determined coupling flow cytometry, fluorescence analysis, and Coulter Counter taking advantage of the fluorescent RhB covalently bonded to the polymer to identify NPs, as recently reported [8]. The flow cytometry gives as output the frequency distribution of cellular fluorescence within the cell population under exam, thus providing additional valuable information on inter-cell variability of cellular uptake compared to the plate fluorimetry which, on the contrary, provides only the average fluorescence of the measured cells. On the other hand, flow cytometric fluorescence scale needs to be calibrated to reach a quantitative estimation of the number of internalized NPs. For this purpose, the average cell fluorescence obtained by flow cytometry was compared to average amount of Rhb per cell, measured with plate fluorimetry. By plotting together the data obtained using different NP concentrations of all NP types, we observed a strong linearity between plate fluorimetry and flow cytometry measurements [8]. Such calibration of the flow cytometric fluorescence scale into absolute numbers of RhB molecules or NPs per cell allowed us to exploit the additional features of this technique for quantitative measures of NP uptake.

The average cellular fluorescence was calculated and subtracted by the average auto-fluorescence measured in samples without NPs, to obtain a relative measure of RhB-associated fluorescence and thus of NP uptake in each sample. The quantification of internalized NPs was obtained by converting the fluorescence signal into the corresponding number of NPs derived by the microplate reader calibration. In the following paragraphs the details of microplate reader and flow cytometric measurements are reported.

2.4. Analysis of NP fluorescence with microplate reader

NPs colloidal suspensions at different concentrations were obtained with serial dilution in PBS, and 300 μl/well of suspension was put in triplicate in a 96-well plate for microplate reader analysis of fluorescence signals. The analysis of fluorescence signals was performed using a multimode microplate reader Infinite® M200 (TECAN, Switzerland) with the following instrumental setting: λ_{exc} 530 nm, λ_{em} 585 nm and gain 100. Instrument response was reproducible within 2% error. The fluorescence signal detected by the instrument was plotted as a function of the number of RhB molecules in each well, derived considering the concentration in the batch and the dilutions applied. Fluorescence was proportional to RhB and from the linear fit of the data we derived the quantity of RhB (pmol) that corresponds to a fluorescence unit detected by the microplate reader in the fixed instrumental setting (see SI) which was finally related to the number of NPs.

2.5. Flow cytometric analysis of NPs

Flow cytometric analysis was performed using a FACS Calibur flow cytometer (Becton Dickinson, USA) acquiring at least 5000 cells in each sample. RhB was excited using an argon laser (λ_{exc}: 488 nm) and its fluorescence was detected in the fluorescence channel FL2 (585/42 nm) using a logarithmic amplifier. Dead cells were excluded from the analysis by propidium iodide (PI) staining. For this purpose 1 μg/ml PI in PBS was added to cell suspensions 5 min before flow cytometric analysis. Cells could be divided into different populations: PI impermeable (viable) and PI permeable (dead cells). PI fluorescence (λ_{exc}: 488 nm) was detected in the fluorescence channel FL3 (>670 nm) using a logarithmic amplifier. Despite the partial overlap of PI and RhB fluorescence emissions, correlated detection of FL2 and FL3 enabled a clear separation of signals of dead from viable cells. All samples were run with and without PI to assure the correct positioning of the region of interest for dead cells [8].

3. Results and discussion

3.1. Nanoparticle production

The characteristics of all the NPs adopted in the present study are summarized in Table 1. In this table the NP batch name (according to the nomenclature reported in the previous section), the adopted monomer, the type of the PEG chains and their relative amount related to the monomer constituting the NPs (reported as, the molar ratio between monomer and PEGylated macromonomer, *r*), the surfactant eventually adopted, the NP size, polydispersity index and the ζ potential are reported. In Table 1 NPs are divided into four different groups, depending on their characteristics. The first group is composed by PLA-based NPs, batch from #1 to #3 (#1–#3), characterized by branches with different PLA chain length and consequently different degradation time. These NPs possess the same PEGylation degree and are produced without using any surfactant. The second group is composed by PCL-based NPs. Here, macromonomers with the same MW (*i.e.* HEMA-CL_3) but with different physical characteristics have been produced, aiming to obtain NPs with various PEGylation degrees in terms of amount and length of PEG chains (#4–#6), surface charge (#6–#10), presence and type of emulsifier (#7–#11). In addition batch #12, constituted of PEGylated PMMA is introduced to compare NPs with the same PEGylation degree but with a different bulk material. Since SDS, an highly efficient surfactant adopted in batches #7 and #11 has been demonstrated to be cytotoxic, its removal has been carried out as already reported in literature [33]. The third group collects positively charged NPs obtained through the copolymerization of both MMA and HEMA-CL_3 with the surfmer HEMA-Ch without using other surfactants. These NPs possess a significant amount of positive charges distributed along their surface as detectable from their positive ζ potential; leading to a family of NPs that can be adopted as suitable carriers for polyanions-delivery such as siRNA [34]. These NPs have tunable size and are based on different raw materials from biodegradable PCL (#13–#15) to biocompatible PMMA (#16–#18). Finally, in the fourth group biocompatible PMMA NPs possessing well controlled size (50, 100, and 200 nm) and with both positive and negative charged surfaces obtained adopting differently charged initiators and biocompatible emulsifier (Tween80) are reported (#19–#24).

Table 1
Characteristics of the NPs involved in the present study.

#	Batch name	Monomer	PEGylation	r^a	Surfactant/Surfmer	Size (nm)	Polydispersity index (–)	ζ potential (mV)
PLA-based								
1	LA6	HEMA-LA_6	HEMA-PEG_{19}	1/8	–	130	0.202	−0.49
2	LA8	HEMA-LA_8	HEMA-PEG_{19}	1/8	–	119	0.119	−5.23
3	LA10	HEMA-LA_{10}	HEMA-PEG_{19}	1/8	–	95.1	0.158	−4.42
PCL-Based								
4	CL3-PEG19-8	HEMA-CL_3	HEMA-PEG_{19}	1/8	–	131	0.176	−2.73
5	CL3-PEG19-16	HEMA-CL_3	HEMA-PEG_{19}	1/16	–	151	0.004	−2.61
6	CL3-PEG9-8	HEMA-CL_3	HEMA-PEG_9	1/8	–	369	0.226	−3.71
7	CL3-SDS	HEMA-CL_3	–		SDS	95.9	0.032	−29.5
8	CL3-PEG19-Ch	HEMA-CL_3	HEMA-PEG_{19}	1/8	Ch 2%	132	0.220	4.42
9	CL3-PEG9-Ch	HEMA-CL_3	HEMA-PEG_9	1/20	Ch 2%	78.8	0.127	26.9
10	CL3-PEG9-Tw	HEMA-CL_3	HEMA-PEG_9	1/20	Tween80	227	0.103	−18.7
11	CL3-PEG9-SDS	HEMA-CL_3	HEMA-PEG_9	1/20	SDS	110	0.11	−19.2
12	MMA-PEG	MMA	HEMA-PEG_{19}	1/8	–	249	0.123	−5.21
Positively charged NPs (PMMA and PCL based)								
13	MMA-1Ch	MMA	–	–	Ch 1%	93.0	0.028	53.8
14	MMA-5Ch	MMA	–	–	Ch 5%	38.5	0.033	56.2
15	MMA-10Ch	MMA	–	–	Ch 10%	23.9	0.082	54.4
16	CL3-1Ch	HEMA-CL_3	–	–	Ch 1%	188	0.016	51.5
17	CL3-5Ch	HEMA-CL_3	–	–	Ch 5%	106	0.076	48.8
18	CL3-10Ch	HEMA-CL_3	–	–	Ch 10%	68.5	0.130	69.2
PMMA based NPs								
19	MMA-50+	MMA	–	–	Tween80	50.2	0.127	34.5
20	MMA-100+	MMA	–	–	Tween80	95.7	0.095	34.9
21	MMA-200+	MMA	–	–	Tween80	188	0.026	8.6
22	MMA-50-	MMA	–	–	Tween80	53.6	0.076	−26.2
23	MMA-100-	MMA	–	–	Tween80	94.8	0.064	−26.9
24	MMA-200-	MMA	–	–	Tween80	196	0.107	−42.5

[a] *r* represents the molar ratio between monomer and PEGylated macromonomer.

3.2. Cellular uptake at 24 h

The results obtained from cellular uptake studies after 24 h of incubation with different concentrations of all the considered NPs are collected in Fig. 1 where the number of internalized NPs is reported as a function of the particle size in a bi-logarithmic plot. Fig. 1a shows a clear linear trend between the number of internalized NPs and their size. This trend seems to be independent of all the NPs features discriminating one NP from the others. More in detail, a larger number of smaller NPs is internalized into cells, ranging from billions for 30 nm NPs to few hundreds for bigger ones (#6, 369 nm). Although the endocytosis process occurs through various mechanisms [5], the observable dependence on the size is in agreement with results reported by Massignani et al. for polymersomes [6], thus verifying that smaller NPs (diameter lower than 100 nm) are easily internalized by cells [11,13,35]. Then, in Fig. 1a a straight line with slope *m*, calculated as equal to −3.233, representing the best data fitting is reported. Further experiments were performed in order to study the effect of one single parameter (*i.e.* the NP size) and avoiding the side effect due to the multivariate analysis presented in Fig. 1a. Several PMMA (#A–#F) and PCL_3-based NPs (#G–#J) with different size were produced trying to reduce the impact of others parameters. No PEGylation was introduced and the same initiator (KPS) and surfactant (Tween80) were used. NPs with different size were obtained only by changing the amount of the emulsifier and the feeding mode as reported in the SI section where the characteristics of the produced NPs are collected (see Table S4). Such NPs were incubated with 4T1 cells for 24 h as reported in the experimental section. In order to reduce the variability of the effect of the concentration, the cells were incubated with the same NP concentration equal to 0.2 mg/mL. The results, expressed as mean number of internalized NPs per cell (#NPs/cell) *versus* the size are reported in Fig. 1b for both PMMA and PCL_3-based NPs. A strict linear relationship between the amount of internalized NPs and the particle size can be observed. Moreover the slope of the curves (*m*) are very similar to the value obtained collecting all the data (Fig. 1a). While the slope of the fitting line is very similar, the intercept of the curves is different and characterizes the different material composing the NPs. Using the value obtained from Fig. 1a, which can be considered as a function of the cell line, different curves simulating the average number of NPs, the area and the polymer volume internalized in each cell are reported in Fig. 1c–e. In addition, other curves with different slopes (*m*) are reported, mimicking other possible behaviors of the system. Fig. 1d shows that at high absolute values of *m*, as the case reported in the present work, smaller NPs bring with them a significantly higher surface area compared to the larger ones, making the smallest NPs ideal carriers for active compounds attached to the NP surface (*e.g.* si-RNA). Conversely, in the case of low absolute value of *m*, larger NPs allow to transport into cells a higher polymer amount, making such NPs good candidates to maximize the delivery of drugs loaded into the NPs.

Then, we moved to analyze the effect of NP concentration on the cellular uptake process. As an example, two groups of NPs with different materials and size were selected. Fig. 2a shows the NP uptake as a function of NP concentration for surfactant free NPs (stabilized and functionalized with the HEMA-Ch) both biodegradable and non-biodegradable (#13–#18) while Fig. 2b correlates the same properties for PMMA NPs obtained adopting Tween80 as emulsifier (#19–#24). Fig. 2a clearly show that, as expected, the higher the NP concentration incubated with cells, the higher the number of internalized NPs. More in detail, although batches #13–#18 possess different characteristics in terms of size, number of positive charges, and starting material (see Table 1) the number of internalized NPs is strictly dependent on their concentration, as detectable from the linear trend evidenced in the bi-logarithmic plot. Fig. 2b shows the same bi-logarithmic plot correlating the number of internalized NPs and their concentration for batches #19–#24. These PMMA-based NPs, with different size and surface charge, show an internalization which is linearly dependent

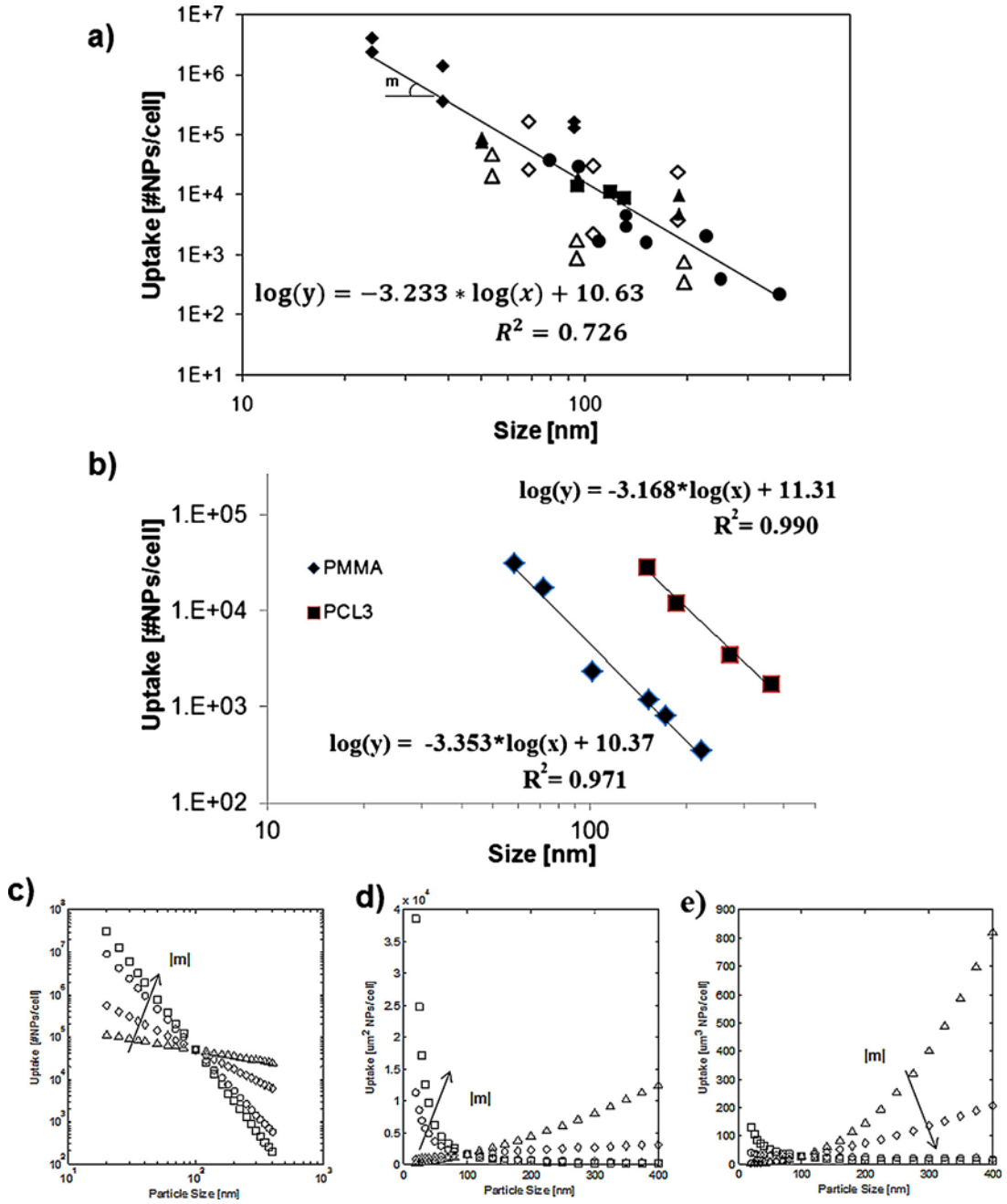

Fig. 1. (a) Number of internalized NPs after 24 h of incubation with 4T1 cells as a function of NP diameter for: PLA-based NPs (□, #1–#3), PCL-based NPs (□, #4–#12), PMMA-based NPs functionalized with HEMA-Ch (□, #13–#15), PCL-based NPs functionalized with HEMA-Ch (♦, #16–#18), PMMA NPs positively (□, #19–#21) and negatively (△, #22–#24) charged produced adopting Tween80. Solid line represents the best fitting of all data while *m* represents the slope of the line. (b) Number of internalized NPs after 24 h of incubation with 4T1 cells as a function of NP diameter for: PMMA NPs (□, #A–#F), PCL-based NPs (□, #G–#J). Solid lines represent the best fitting of all data. (c) Simulation of the number of internalized NPs *versus* their diameter for different values of *m*: −4 (□), −3.233 (value obtained from Fig. 1a, (○ −1.5 (♦) and −0.5 (Δ). (d) Internalized NP area *versus* NP diameter and (e) internalized NP volume *versus* NP diameter for different *m* values.

on the NP concentration, as recently reported by Seo et al. [36] Moreover, a clear dependence of other characteristics (such as size and charge surface) is also detectable; in fact smaller and positively charged NPs are internalized more efficiently compared to both the negatively charged and the ones with diameter larger than 100 nm. Furthermore, the number of internalized NPs increases with their concentration without joining a plateau, at least for the considered experimental conditions. In this analysis higher concentrations were not considered since they significantly affect cell proliferation. Therefore, aiming to elucidate the kinetic of the NP internalization, the uptake of four different batches of NPs was monitored from 2 to 24 h as shown in Fig. 3. The four batches possess similar size, around 100 nm, and they were selected to test different materials and surface charges. In Fig. 3 the kinetic of internalization of NPs with a comparable size (around 100 nm, batches #3, #4, #20 and #23) at two labeling concentrations named as high (H) and low (L) is reported. In the case of lower concentrations the number of internalized NPs is substantially constant during the time, meaning that NPs are successfully internalized reaching a sort of steady-state as reported by Seonen et al. for magnetoliposomes [37]. Conversely, for higher concentrations after a fast uptake, imputable to the high external NP concentration (former

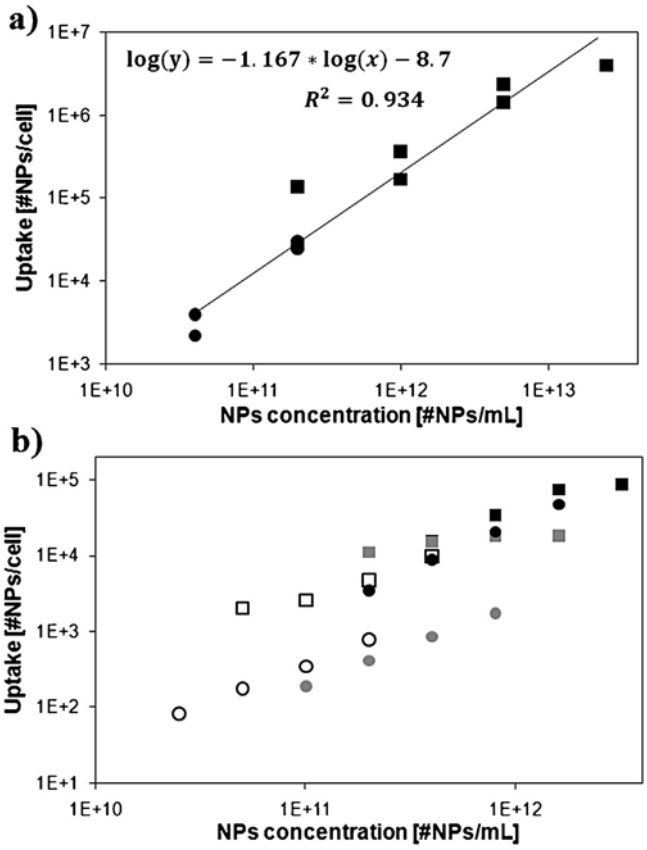

Fig. 2. Number of internalized NPs after 24 h of incubation with 4T1 cells at different NP concentration for: (a) PMMA NPs functionalized with HEMA-Ch (□, #13–#15) and PCL-ones (□, #16–#18). Solid line represents the best fitting of all data; (b) PMMA NPs positively (□, □, □ for 50, 100, and 200 nm respectively, #19–#21) and negatively (□, □, ○ for 50, 100, and 200 nm respectively, #22–#24) charged produced with Tween80.

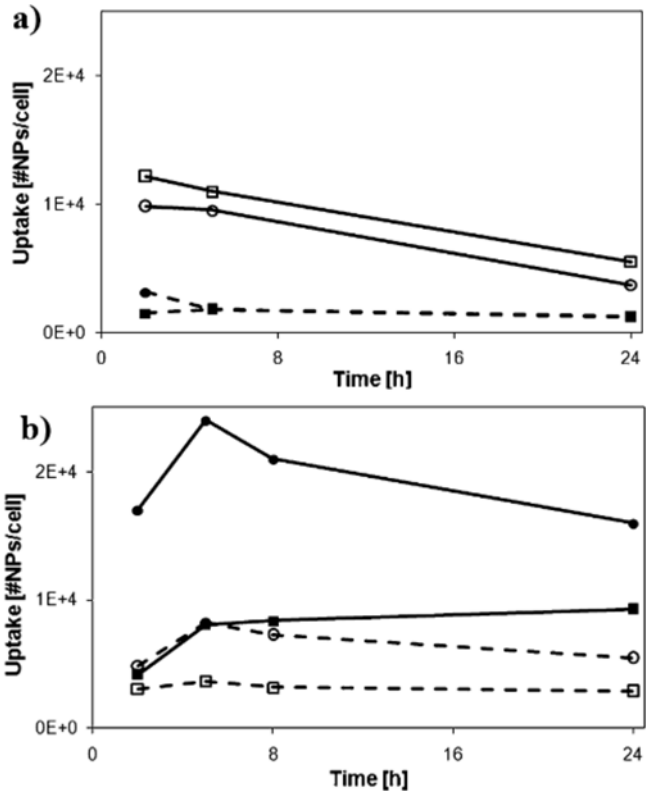

Fig. 3. Kinetic of NP internalization in 4T1 cells incubated with: (a) batch #3 at 1E+12 NPs/mL (□, high concentration – H) and 2E+11 (□, low concentration, L); batch #4 at 1E+12 NPs/mL (○, H) and 2E+11 NPs/mL (□, L); (b) batch #20 at 16E+11 NPs/mL (□, H) and 4E+11 (□, L); batch #23 at 4E + 11 NPs/mL (○, H) and 1E+11 NPs/mL (□, L).

2–4 h), the number of NPs into cells decreases, suggesting that there is an active cellular elimination process. Fig. 3a also shows that PEGylated NPs with similar size possess similar uptake characteristics independently on the starting material. Conversely, significant differences are detectable for the uptake of PMMA-based NPs with different surface charge as reported in Fig. 3b. Positively charged NPs show a relevant fast uptake in the first hours, followed by a slow exit of NPs during the next 24 h. On the contrary, a lower number of negatively charged NPs is internalized, without an evidence of enhanced internalization in the first hours of incubation. Reported results highlight the paramount role played by the surface charge in the internalization process as already reported in the literature [17,30]. In addition the role of the surface charge in the internalization is presented in Fig. 4a, where the volume of different NPs (all those listed in Table 1) internalized into cells at different NPs concentration is reported. In Fig. 4a it is possible to observe that the total volume of internalized polymer is not strictly dependent upon NP concentration. Consequently, a higher NP concentration, which generally means a larger number of internalized NPs (Fig. 2), does not necessarily mean a higher volume of polymer internalized to cell as reported in Fig. 1e for NP with different sizes. Nevertheless NPs can be divided in three different groups depending upon their surface charge; the upper region in Fig. 4a (internalized volume of polymer higher than 15 $[\mu m]^3$) contains only NPs with positive surface charge, confirming the enhanced uptake efficiency of these NPs. On the contrary, the lower region of Fig 4a, delimiting internalized polymer volume lower than 3 $[\mu m]^3$, contains only negatively charged NPs. Finally, the intermediate region (between 3 and 15 $[\mu m]^3$) contains NPs with various ζ potential from positive to negative as well as neutral (around 0 mV), typical of NPs possessing a strong PEGylation degree. In this case it appears that PEGylation does not significantly decrease the uptake if compared to the effect of negative charges. This result is quite expected since the negative charge of the phospholipids constituting the cellular membrane has a repulsive effect for the negatively charged NPs [38,39].

The kinetic of NP exit from cells was also studied in order to further elucidate the effect of the surface charge on cell ability to retain NPs. After 24 h of incubation, cell medium containing NPs was replaced with NP-free medium and the NP amount retained into cells was monitored at different times (washout). Fig. 4b shows the relative amount of NPs which remain into cells 24 h after the washout for samples #3 and #4. An amount ranging from 40 to 70% of the internalized NPs is localized into cells 24 h after the washout, independently of the starting NP concentration, suggesting that, in agreement with the literature, only this fraction of PEGylated biodegradable NPs is definitely retained by cells [35,40]. The percentage of NPs remaining into the cells 24 h after washout is presented in Fig. 4c for 4 batches of NPs with similar dimension (batches #3, #4, #20, and #23). As revealed from internalization kinetic experiments (see Fig. 3, in which the same NP batches were adopted) positively charged NPs are trapped into cells in a more efficient way, while the negative ones easily leave cells. Finally, it is worth noticing that an intermediate effect was obtained for PEGylated NPs, both for PLA and PCL-based ones. Reported results clearly show that the PEGylation, usually adopted to reduce opsonization in *in vivo* applications does not enhance the NPs internalization [38,41], but hinders the NP exit from cells. As NP retention studies were performed exposing the cells to sub-toxic NP concentrations,

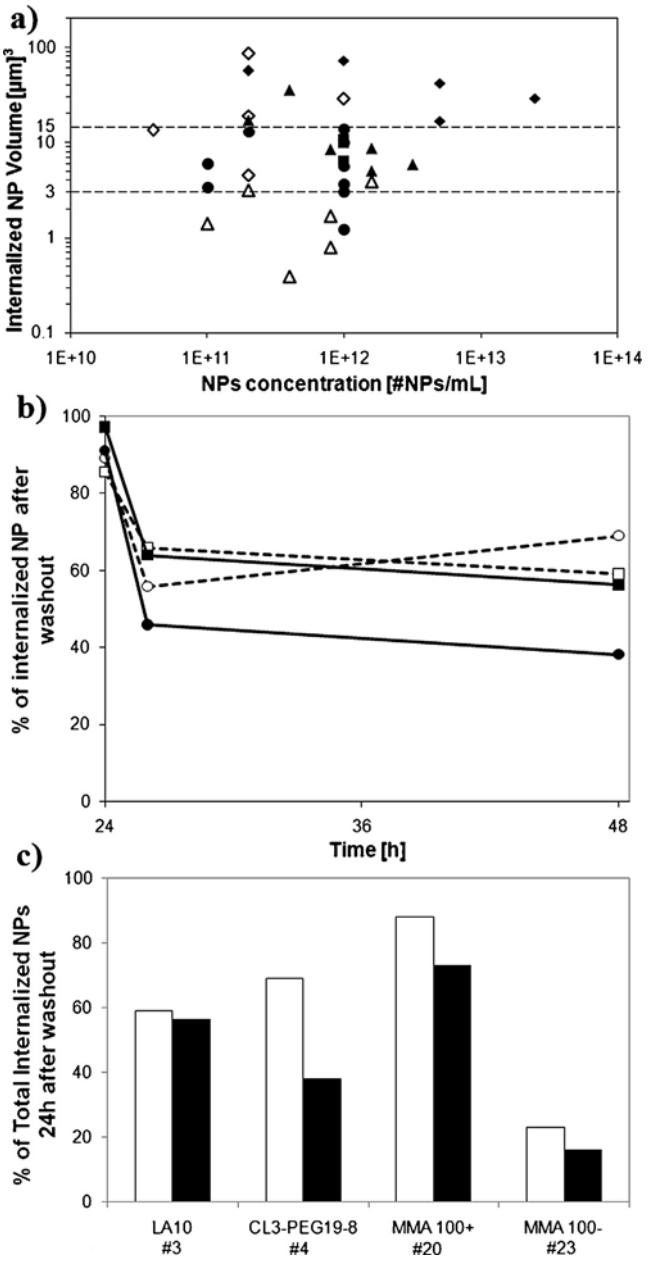

Fig. 4. (a) Internalized volume of NPs after 24 h of incubation with 4T1 cells as a function of NP concentration for: PLA-based NPs (□, #1–#3), PCL-based NPs (□, #4–#12), PMMA-based NPs functionalized with HEMA-Ch (□, #13–#15), PCL-based NPs functionalized with HEMA-Ch (♦, #16–#18), PMMA NPs positively (□, #19–#21) and negatively (Δ, #22–#24) charged produced with Tween80. (b) Kinetics of NP exit from cells for: batch #3 at 1E+12 NPs/mL (□, H) and 2E+11 (□, L), batch #4 at 1E+12 NPs/mL (□, H) and 2E+11 NPs/mL (○, L). (c) Percentage of NPs remaining into cells 24 h after the NP washout at L (white bars) and H (black bars) NP concentration (same concentrations adopted in Fig'. 3).

it is possible to exclude that the kinetics of NP exit was influenced by the occurring of cell death (further details are reported in the SI section: "4.5 Effect of cell viability over retention data").

The uptake of surfactant free NPs based of HEMA-CL_3 with different PEGylation degree obtained using different amount (r equal to 1/8 or 1/16) or length (9 or 19 of ethylene glycol) of PEG chains (batches #4–#8) along with their effect on cell proliferation after 24 h of incubation with 4T1 cells, are shown in Fig. 5a and b. Fig. 5a shows that the internalized volume of NPs for batches #4–#6 and #8 is comprised between 3 and 6 $[\mu m]^3$, in the intermediate region depicted in Fig. 4a; suggesting that, once PEG chains cover the NPs surface (as evaluable from the ζ potential values close to 0 mV, Table 1) there are no significant differences in terms of NP uptake by increasing the PEG content. Moreover, a larger number of internalized NPs is revealed for non PEGylated NPs (#7) stabilized adopting SDS. Furthermore, cell viability shown in Fig. 5b demonstrates that incubation with all of these NPs, except for batch #6, does not induce a significant impairment in cell proliferation. Despite PEGylated NPs are not so effective in terms of internalized volume into cells, they can be considered as suitable carriers, since the differences with positively charged NPs in terms of mass of internalized polymer are lower than one order of magnitude. This finding is in agreement with the literature where only PEG chains with MW higher than 2000 Da have been found to substantially reduce the uptake [42].

Usually an emulsifier is adopted for both NPs production and stabilization, and, in the next part of this work, its effects on the NP toxicity are discussed. Three NP batches with the same PEG chains of batch #6 (HEMA-PEG_9) have been produced adopting the following surfactants: HEMA-Ch as a positive surfmer (#9), Tween80 (#10), and SDS (#11). The latter is an efficient anionic surfactant removed after NPs synthesis due to its potential toxicity and substituted with Tween80, as reported in Section 2. A reduced cytotoxic effect is observed only in the case of NPs in which the surfactant is covalently bound to the polymer matrix (*i.e.* HEMA-Ch, batch #9), suggesting that a surfactant adsorbed on the NP surface, as Tween80, affects cell proliferation. However, such effects are negligible at longer incubation time or lower NP concentration (see SI). Furthermore the presence of an emulsifier implies the lack of the screening effect of PEG chains, thus leading to a change of the NP ζ potential, from values close to 0 mV to −20 mV (see Table 1), and to an increase of the overall NP uptake (up to 12 $[\mu m]^3$ for batch #10). A further comparison was also done between surfactant free NPs with the same PEGylation degree (HEMA-PEG_{19}, r = 1/8), produced with different materials and/or different MW polymers. In detail, NPs based on PCL or biocompatible PMMA (batch #4 and #12) and PLA with higher MW (batches #1–#3) were considered and the average number of internalized NPs for each cell after 24 h of incubation, as well as NP toxicity are shown in Fig. 5c and d. Fig. 5c shows that an increase in the MW of the polymer branched chains, from the methyl group of MMA, moving to 3 units of PCL and to 6, 8, and 10 units for PLA, leads to an increased number of internalized NPs, in agreement with finding of Lorenz et al. for different methacrylates with different length of the side chains [23,43]. Finally, it has been found that all the considered NPs do not affect cell proliferation, excluding non-biodegradable PMMA-based NPs as reported in Fig. 5d.

As a final part of this work, all the biodegradable NPs investigated have been listed taking into account both the NP uptake efficiency and their toxicity in order to establish a criterion to characterize the efficacy of polymer NPs as drug delivery carriers. In Fig. 6 cellular uptake of biodegradable NPs #1–#11 and #16–#18 are summarized, in particular, the uptake efficiency evaluated in terms of internalized volume of NPs is compared to the cell viability. The left panel in Fig. 6 delimits NPs that significantly impair cell proliferation, determined as a cut off equal to 80% for cell viability compared to the control. In this panel are placed the biggest NPs (diameter larger than 300 nm), those with the surfactant adsorbed on the NP surface, and those positively charged. In the right panel NPs that do not show evident cytotoxicity are listed. In the work of Salvati et al. an average uptake of 20,000 poly(styrene)-NPs per cell was estimated after a short incubation time [44]. Since this value is recognized as satisfactory for drug delivery application we selected the same value, evaluated as an internalized polymer volume per cell, as a reference to delimit the upper region containing NPs whit the best uptake performances. In this region PLA (#1–#3), and PCL-based NPs are placed (#4, #7, #9). Finally, in the lower-right region

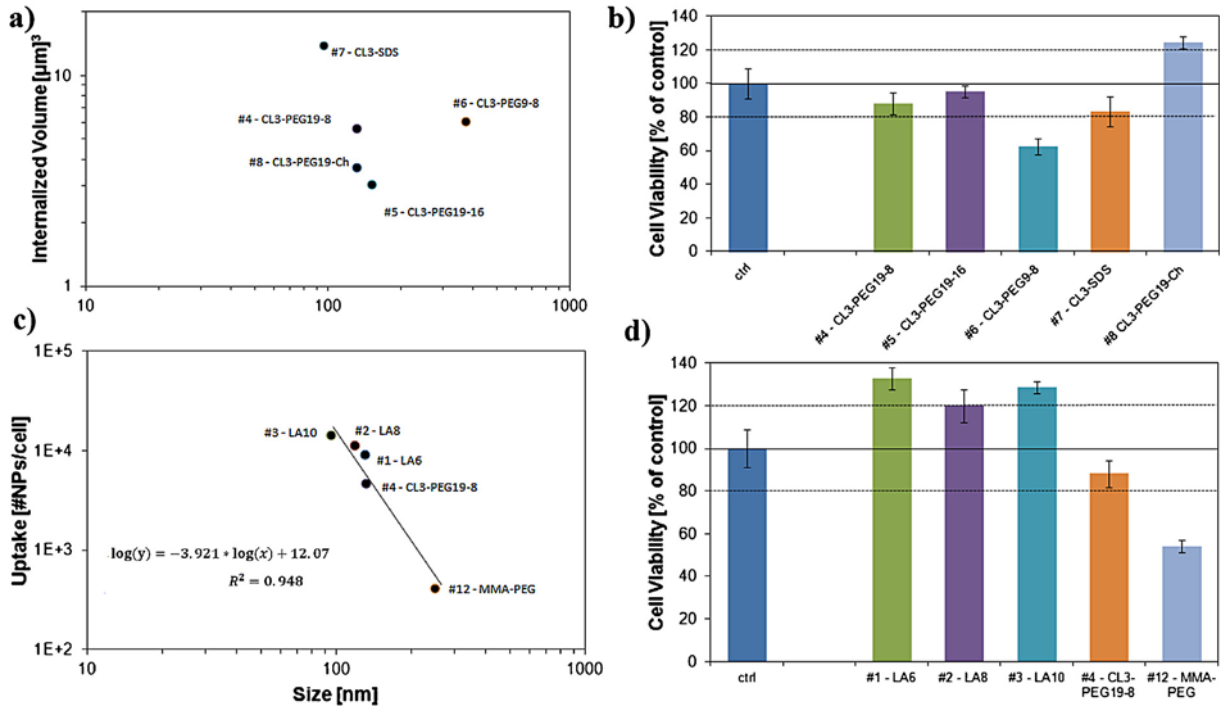

Fig. 5. (a) Internalized volume of NP for batches #4–#8 after 24 h incubation with 4T1 cells as a function of NPs diameter. (b) Assessment of cell proliferation of 4T1 cells exposed for 24 h to different PEGylated NPs. (c) Number of internalized NP for batches #1–#4 and #12 after 24 h of incubation with 4T1 cells as a function of NP diameter. (d) Cell viability determined by cell counting after 24 h of incubation with NPs.

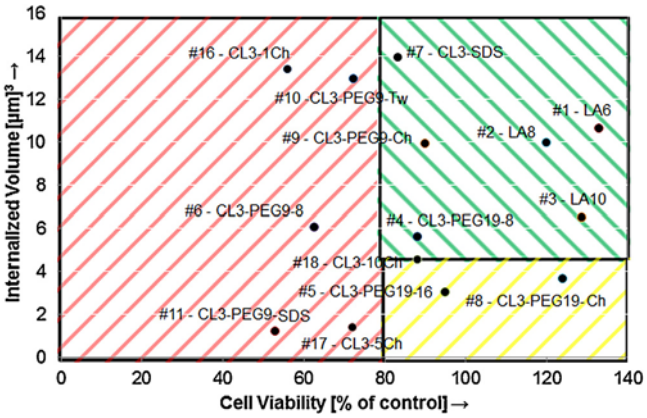

Fig. 6. NP selection depending on their antiproliferative effect (24 h incubation in 4T1 cells) and the uptake efficiency evaluated in terms of internalized volume of NPs into 4T1 cells.

are collected NPs with an internalized polymer volume lower than the adopted reference value, this area mainly collects NPs with various PEGylation degrees which do not significantly impair cell proliferation. It is important to point out that NPs present in the lower right panel, although not efficiently internalized, are suitable for further studies since do not have significant effects over cell proliferation. The reported results are related to the materials selected for the NP synthesis as well as the type cell line; however we are confident that this procedure can be extended to different NPs and can be considered a good tool to evaluate the possible use of polymer NPs as drug delivery vehicles.

4. Conclusions

Numerous NPs with different size, surface charge, PEGylation degree, and adopted emulsifier have been synthesized using different polymers and NP uptake in 4T1 cells has been investigated allowing the evaluation of the number of internalized NPs in each cell and to enable a comparison of the efficiency among different NP formulation as potential drug carrier. As a first result, a linear relationship between uptake and NP size, independent of all the other NP features, was found. An analog relationship was also found between the number of internalized NPs and their concentration and it is extended to evaluate the area and the volume internalized per NP size. Such effect was also evaluated at shorter incubation time, suggesting that there is a limit to the number of NPs internalized by cells. The effect of surface charge was also evaluated, finding that positive charges promote the uptake and further NP cellular restrain for longer time. Adopted polymer constituting the NPs, PEGylation degree, and the use of different emulsifiers were also investigated allowing establishing a criterion, coupling the uptake and the cytotoxicity, to select NPs with the best *in vitro* performances as drug delivery carriers. For the materials selected in this work it was found that hydrophobic PLA-based NPs with higher MW possess the optimal characteristics for the uptake into cells. PEGylation reduces the internalization efficiency but do not affect cell growth, as a result, PEGylated PCL-based NPs seems to be suitable for further studies.

Acknowledgments

We acknowledge support from AIRC Special Program Molecular Clinical Oncology “5 per mille”. We also acknowledge the European Center for Nanomedicine (CEN) for the purchase of chemicals.

Appendix A. Supplementary data

Supplementary data associated with this article can be found, in the online version

References

[1] R. Zhou, H.Y. Zhou, B. Xiong, Y. He, E.S. Yeung, J. Am. Chem. Soc. 134 (2012) 13404–13409.
[2] J.A. Kim, C. Aberg, A. Salvati, K.A. Dawson, Nat. Nanotechnol. 7 (2012) 62–68.
[3] L. Treuel, X.E. Jiang, G.U. Nienhaus, J. R. Soc. Interface 10 (2013).
[4] V. Mailaender, K. Landfester, Biomacromolecules 10 (2009) 2379–2400.
[5] I. Canton, G. Battaglia, Chem. Soc. Rev. 41 (2012) 2718–2739.
[6] M. Massignani, C. LoPresti, A. Blanazs, J. Madsen, S.P. Armes, A.L. Lewis, G. Battaglia, Small 5 (2009) 2424–2432.
[7] T. dos Santos, J. Varela, I. Lynch, A. Salvati, K.A. Dawson, Small 7 (2011) 3341–3349.
[8] R. Ferrari, M. Lupi, F. Falcetta, P. Bigini, K. Paolella, F. Fiordaliso, C. Bisighini, M. Salmona, M. D'Incalci, M. Morbidelli, D. Moscatelli, P. Ubezio, Nanotechnology 25 (2014) 045102.
[9] H. Kettiger, A. Schipanski, P. Wick, J. Huwyler, Int. J. Nanomed. 8 (2013) 3255–3269.
[10] M. Elsabahy, K.L. Wooley, Chem. Soc. Rev. 41 (2012) 2545–2561.
[11] C. He, Y. Hu, L. Yin, C. Tang, C. Yin, Biomaterials 31 (2010) 3657–3666.
[12] C. Freese, M.I. Gibson, H.A. Klok, R.E. Unger, C.J. Kirkpatrick, Biomacromolecules 13 (2012) 1533–1543.
[13] J.A. Varela, M.G. Bexiga, C. Aberg, J.C. Simpson, K.A. Dawson, J. Nanobiotechnol. 10 (2012).
[14] C.D. Walkey, J.B. Olsen, H.B. Guo, A. Emili, W.C.W. Chan, J. Am. Chem. Soc. 134 (2012) 2139–2147.
[15] S.S. Yu, C.M. Lau, S.N. Thomas, W.G. Jerome, D.J. Maron, J.H. Dickerson, J.A. Hubbell, T.D. Giorgio, Int. J. Nanomed. 7 (2012) 799–813.
[16] Y. Hu, J. Xie, Y.W. Tong, C.-H. Wang, J. Control. Release 118 (2007) 7–17.
[17] S. Bhattacharjee, D. Ershov, K. Fytianos, J. van der Gucht, G.M. Alink, I. Rietjens, A.T.M. Marcelis, H. Zuilhof, Particle Fibre Toxicol. 9 (2012).
[18] A. Musyanovych, J. Dausend, M. Dass, P. Walther, V. Mailaender, K. Landfester, Acta Biomater. 7 (2011) 4160–4168.
[19] L. Florez, C. Herrmann, J.M. Cramer, C.P. Hauser, K. Koynov, K. Landfester, D. Crespy, V. Mailander, Small 8 (2012) 2222–2230.
[20] A. Schrade, V. Mailander, S. Ritz, K. Landfester, U. Ziener, Macromol. Biosci. 12 (2012) 1459–1471.
[21] J.C. Sunshine, D.Y. Peng, J.J. Green, Mol Pharmaceut. 9 (2012) 3375–3383.
[22] A. Hocherl, M. Dass, K. Landfester, V. Mailander, A. Musyanovych, Macromol. Biosci. 12 (2012) 454–464.
[23] S. Lorenz, C.P. Hauser, B. Autenrieth, C.K. Weiss, K. Landfester, V. Mailaender, Macromol. Biosci. 10 (2010) 1034–1042.
[24] M. Dossi, R. Ferrari, L. Dragoni, C. Martignoni, P. Gaetani, M. D'Incalci, M. Morbidelli, D. Moscatelli, Macromol. Mater. Eng. 298 (2013) 771–778.
[25] T. Tenuta, M.P. Monopoli, J. Kim, A. Salvati, K.A. Dawson, P. Sandin, I. Lynch, PLoS ONE 6 (2011).
[26] R. Ferrari, Y.C. Yu, M. Morbidelli, R.A. Hutchinson, D. Moscatelli, Macromolecules 44 (2011) 9205–9212.
[27] Y. Yu, R. Ferrari, M. Lattuada, G. Storti, M. Morbidelli, D. Moscatelli, J. Polym. Sci. A: Polym. Chem. 50 (2012) 5191–5200.
[28] S. Papa, F. Rossi, R. Ferrari, A. Mariani, M. De Paola, I. Caron, F. Fiordaliso, C. Bisighini, E. Sammali, C. Colombo, M. Gobbi, M. Canovi, J. Lucchetti, M. Peviani, M. Morbidelli, G. Forloni, G. Perale, D. Moscatelli, P. Veglianese, ACS Nano 7 (2013) 9881–9895.
[29] R. Ferrari, C. Colombo, C. Casali, M. Lupi, P. Ubezio, F. Falcetta, M. D'Incalci, M. Morbidelli, D. Moscatelli, Int. J. Pharm. 453 (2013) 551–559.
[30] M.R. Lorenz, V. Holzapfel, A. Musyanovych, K. Nothelfer, P. Walther, H. Frank, K. Landfester, H. Schrezenmeier, V. Mailander, Biomaterials 27 (2006) 2820–2828.
[31] K. Tao, M. Fang, J. Alroy, G.G. Sahagian, BMC Cancer 8 (2008).
[32] R. Ferrari, Y. Yu, M. Lattuada, G. Storti, M. Morbidelli, D. Moscatelli, Macromol. Chem. Phys. 213 (2012) 2012–2018.
[33] R. Ferrari, C. Colombo, M. Dossi, D. Moscatelli, Macromol. Mater. Eng. 298 (2013) 730–739.
[34] L. Dragoni, R. Ferrari, M. Lupi, F. Falcetta, P. Ubezio, L. Sitia, P. Bigini, M. Salmona, M. D'Incalci, M. Morbidelli, D. Moscatelli, Nanoscale (2014), submitted.
[35] T.G. Iversen, T. Skotland, K. Sandvig, Nano Today 6 (2011) 176–185.
[36] J.H. Seo, K. Cho, S.Y. Lee, S.W. Joo, Nanotechnology 22 (2011).
[37] S.J.H. Soenen, E. Illyes, D. Vercauteren, K. Braeckmans, Z. Majer, S.C. De Smedt, M. De Cuyper, Biomaterials 30 (2009) 6803–6813.
[38] F. Alexis, E. Pridgen, L.K. Molnar, O.C. Farokhzad, Mol. Pharmaceut. 5 (2008) 505–515.
[39] K. Xiao, Y. Li, J. Luo, J.S. Lee, W. Xiao, A.M. Gonik, R.G. Agarwal, K.S. Lam, Biomaterials 32 (2011) 3435–3446.
[40] A. Vollrath, A. Schallon, C. Pietsch, S. Schubert, T. Nomoto, Y. Matsumoto, K. Kataoka, U.S. Schubert, Soft Matter 9 (2013) 99–108.
[41] J.L. Perry, K.G. Reuter, M.P. Kai, K.P. Herlihy, S.W. Jones, J.C. Luft, M. Napier, J.E. Bear, J.M. DeSimone, Nano Lett. 12 (2012) 5304–5310.
[42] V.C.F. Mosqueira, P. Legrand, A. Gulik, O. Bourdon, R. Gref, D. Labarre, G. Barratt, Biomaterials 22 (2001) 2967–2979.
[43] Y. Chen, S. Sajjadi, Polymer 50 (2009) 357–365.
[44] A. Salvati, C. Aberg, T. dos Santos, J. Varela, P. Pinto, I. Lynch, K.A. Dawson, Nanomed.–Nanotechnol. Biol. Med. 7 (2011) 818–826.